Fuel 401 (2025) 135851

Contents lists available at ScienceDirect

Fuel

journal homepage: www.elsevier.com/locate/fuel

Full Length Article

Turbulent flame characteristics of ethane and blends with hydrogen

Jinzhou Li, Junfeng Yang *

School of Mechanical Engineering, University of Leeds, Leeds LS2 9JT, United Kingdom

ARTICLE INFO

Keywords:
Turbulent expanding flame
Ethane/hydrogen/air
Turbulent burning velocity correlation
Karlovitz stretch factor

ABSTRACT

Ethane, a critical component of natural gas and a significant fuel source, presents a notable knowledge gap regarding its turbulent flame characteristics. This study employs the Leeds MK-II fan-stirred, spherical combustion vessel to explore the impact of pressure, temperature, turbulence intensity and hydrogen additions on ethane/air premixed flames. Experimental measurements span a broad range, encompassing equivalence ratios from 0.8 to 1.2, rms turbulent velocity at 1, 3, and 5 m/s, pressures of 0.1 and 0.5 MPa, temperatures at 300 and 360 K, and hydrogen additions varying from 25 % to 100 % by volume fraction. This study's measurements are plotted on Peters-Borghi turbulent combustion diagram, covering the wrinkled flamelets, corrugated flamelets, and distributed reaction zones. Results show that both turbulent flame propagation speeds and turbulent burning velocities increase with root-mean-square turbulent velocity (u'), hydrogen additions, temperature, and pressure. A revised *U-K* turbulent burning velocity correlation is proposed by incorporating pressure explicitly as a key variable. This refinement enables separate expressions for different pressure levels and significantly improves predictive accuracy. This advancement allows for a distinct expression for each pressure level, enhancing the accuracy compared to the previous approach that used strain rate Markstein number. A comparison with previous measurements under V-shaped flame configurations shows that, despite differing setups, the relationship between normalized turbulent burning velocity ($\frac{u_{tr}}{u'}$) and the Karlovitz stretch factor (K) remains consistent, confirming the general validity of the proposed correlation.

1. Introduction

Ethane, representing the second-largest component in natural gas with a concentration range of 0.5 % to 13.3 % [1], is of significant industrial importance. Primarily, it serves as a feedstock in the production of ethylene. However, the increasing production of ethane raises concerns about the risk of accidental explosions, particularly due to potential leaks. Recently, ethane has gained attention as a potential fuel for power generation and as an additive to diesel in large marine vessels and engines [2–6]. Its advantages over methane, such as shorter combustion duration, ignition delay time, higher heat release, and stable combustion in lean conditions, make it an attractive alternative [4,5]. Given these applications, understanding the combustion characteristics of ethane/air flames becomes crucial.

Extensive research, including studies by Lowry et al. [7], Mitu et al. [8], Nilsson et al. [9], Ravi et al. [10], Li et al. [11] and Zuo et al. [12,13], has thoroughly reported on the laminar flame characteristics of ethane/air mixtures, focusing on aspects like laminar burning velocities and flame instabilities. Despite a well understanding of laminar flame characteristics, turbulent flame characteristics are equally important for representing practical combustion systems, including gas turbines [14], combustion engines [15,16], burners [17–19] and scenarios involving explosion hazards [20,21]. Particularly, the turbulent burning velocity (TBV), u_t stands out as a crucial parameter in both explosion simulation and engine design [15,20].

Turbulent premixed flames, unlike their laminar counterparts, exhibit enhanced burning rates. This phenomenon is attributed to turbulent eddies, which increase the combustion surface area by wrinkling the flame surface. Numerous experimental studies have explored the influence of turbulence on flame propagation and quantified the turbulent burning velocity. The pioneering study by Abdel-Gayed et al. [22] focused on measuring the TBV for methane/air mixtures across different equivalence ratios in a fan-stirred combustion vessel. In this research, adjustment of the fan's rotational speed was employed to modify the root-mean-square turbulent velocity, u'. It was found that the TBV consistently increases with u'. Lawes et al. [23] further investigated this phenomenon using high-speed Schlieren imaging in a fan-stirred spherical vessel to measure the TBV of methane, methanol, and *iso*-octane under elevated pressures. In related studies, Goulier et al. [24] and

* Corresponding author.
E-mail address: J.Yang@leeds.ac.uk (J. Yang).

https://doi.org/10.1016/j.fuel.2025.135851
Received 14 February 2025; Received in revised form 16 May 2025; Accepted 29 May 2025
Available online 5 June 2025

Nomenclature

A	turbulent flame surface area (m^2)
c	progress variable
Da	Damköhler number, $Da = (l/u')(\delta_l/u_l)$
f	fan speed (rpm)
Ka	Karlovitz number
K	Karlovitz stretch factor, $K = (\frac{u'}{\lambda})/(\frac{u_l}{\delta_l}) = (0.25/Pr)(u'/u_l)^2(u'l/\nu)^{-0.5}$
$\overline{k}_\eta$	dimensionless wave number
$\overline{k}_{\eta G}$	the upper limit wave number, $\overline{k}_{\eta G} = \frac{2\pi\eta}{l_G}$
$\overline{k}_{\eta k}$	the lower limit wave number, $\overline{k}_{\eta k} = \frac{2\pi\eta}{nL} = (\frac{32\pi}{15^{0.25}n})R_\lambda{}^{-1.5}$
R_{et}	turbulent Reynolds number
l_G	Gibson scale (mm), $l_G = 0.133L(\frac{u'}{u_l})^{-3}$
l	integral length scale of combustion vessel (20 mm)
L_b	Markstein length on the burned side of the flame (mm)
Le	Lewis number
Ma_b	Markstein number on the burned side
Ma_{sr}	Markstein number associated to aerodynamic strain
P	pressure (MPa)
Pr	Prandtl number, $P_r = \frac{\nu}{\alpha}$
r_v	reference flame radius based on the volume (mm)
r_{sch}	flame front radius obtained by high-speed Schlieren imaging system (mm)
R_L	turbulent Reynold number based on L, $R_L = \frac{u'L}{\nu}$
R_λ	turbulent Reynold number based on λ, $R_\lambda = \frac{u'\lambda}{\nu}$
S_{sch}	flame propagation speed based on Schlieren flame radius (m/s)
S_s	unstretched laminar flame speed (m/s)
$\overline{S}(\overline{k}_\eta)$	dimensionless power spectral density
T	temperature (K)
U	dimensionless parameter with the ratio of $\frac{u_t}{u_k{}'}$
u'	rms turbulent velocity (m/s)
$u_k{}'$	effective rms turbulent velocity (m/s)
u_l	unstretched laminar burning velocity (m/s)
u_{tr}	turbulent burning velocity based on r_v (m/s)
$u_{tr(30mm)}$	turbulent burning velocity at $r_{sch} = 30$ mm (m/s)
V_{H_2}	hydrogen volume fraction
$V_{C_2H_6}$	ethane volume fraction
X_{H_2}	percentage of hydrogen based on volume

Greek symbols

α	thermal diffusivity (m^2/s) and constant for Eq.7
β	constant
η	Kolmogorov length scale (mm), $\eta = \lambda/(15^{0.25}R_\lambda{}^{0.5})$
δ_l	laminar flame thickness, $\frac{\nu}{u_l Pr}$ (mm)
ν	unburnt gas kinematic viscosity (m^2/s)
λ	Taylor length scale (mm), $\lambda = L(\frac{16}{R_L})^{1/2}$
ρ_u	unburnt gas density (kg/m^3)
ρ_b	burnt gas density (kg/m^3)
σ	thermal expansion ratio, $\sigma = \rho_u/\rho_b$
ϕ	equivalence ratio

Kitagawa et al. [25] applied the same technique to investigate the effects of u' on hydrogen/air flame propagation, reporting that the turbulent flame speed increases as the flame radius expands. Wang et al. [26] investigated ammonia/oxygen/nitrogen mixtures in a fan-stirred vessel, demonstrating that turbulence can significantly enhances the burning rate of low-reactivity fuels such as ammonia.

Adding hydrogen to hydrocarbon fuels is an effective strategy to promote ignition, increase burning velocity, enhance combustion performance, and reduce greenhouse gas emissions [27]. Several studies have investigated the addition of hydrogen to both hydrocarbons and ammonia to better understand its influence on turbulent combustion behaviour. Fairweather et al. [28] employed a combustion vessel to measure the TBV of methane/hydrogen/air mixture and found that the addition of hydrogen to methane significantly enhances the TBV. Beyond methane-based systems, the effects of hydrogen enrichment have also been investigated for other fuels, including *iso*-octane [29], n-heptane [30], and ammonia [31,32], These studies consistently show that hydrogen addition in turbulent premixed flames significantly increases TBV and reduces greenhouse gas emissions, further highlighting the broad applicability of hydrogen enrichment in improving combustion characteristics.

Another important aspect of turbulent premixed flame research is the development of correlations for TBV, which serve as input for source terms in turbulent combustion simulations [20,33]. Numerous correlations have been proposed to describe TBV under varying conditions. Damköhler [34] was the first to report that increasing u' enhances flame front wrinkling and increases the flame surface area. Based on this observation, a direct proportionality was proposed between the turbulent-to-laminar burning velocity (u_t/u_l) and the flame surface area ratio (A/a). Expanding on this concept, Clavin and Williams [35] developed a expression to emphasize the influence of turbulence intensity: $\frac{u_t}{u_l} = 1 + (\frac{u'}{u_l})^2$. Schmid et al. [36] introduced a correlation involving the Damköhler number, Da applicable to a wider range of combustion regimes: $\frac{u_t}{u_l} = 1 + u'/u_l(1 + Da^{-2})^{-1/4}$.

Bradley et al. [37] identified the critical roles of flame stretch rate and Lewis number in TBV and proposed the following correlation: $u_t/u_k{}' = 0.88(KLe)^{-0.3}$, where K is the Karlovitz stretch factor and Le is the Lewis number. The Karlovitz stretch factor is defined as: $K = (\frac{u'}{\lambda})/(\frac{u_l}{\delta_l})$ representing the ratio of turbulent strain rate ($\frac{u'}{\lambda}$) to a laminar flame strain rate ($\frac{u_l}{\delta_l}$) with λ denoting the Taylor microscale and δ_l the laminar flame thickness. In a more recent study, Bradley et al. [38] measured TBV in ethanol/air mixtures at pressures up to 1.2 MPa and u' up to 6 m/s. A new correlation, referred to as the *U-K* correlation, was proposed in the form: $U = \frac{u_t}{u_k{}'} = \alpha K^\beta$, where $u_k{}'$ is the effective root-mean-square turbulent velocity, α and β are function of strain rate Markstein numbers, Ma_{sr}, accounting for the influence of strain rate on TBV. This formulation has subsequently been refined and extended [39] to include over seven different fuels under elevated temperature and pressure conditions up to 1 MPa, demonstrating its broader applicability. However, accurate measurement of Ma_{sr} remains challenging and introduces uncertainty in the practical application of this correlation.

To the best of current knowledge, there is a notable gap in the literature concerning the turbulent flame characteristics of ethane/air mixtures, with the effects of hydrogen addition on turbulent ethane premixed flames remaining unclear. Consequently, measuring the turbulent flame characteristics of ethane/air and ethane/hydrogen/air mixtures is important. The present study is driven by two primary objectives. First, to address this knowledge gap by measuring the influence of turbulence on the propagation of expanding ethane/air and ethane/hydrogen/air flames over a wide range of equivalence ratios, initial temperatures, pressures, and turbulence intensities (u'). Second, the measured TBV data serve as a reference database and, when combined with ethanol data from [38], are used to refine the *U-K* correlation proposed in [39], yielding a strong fit with coefficient of determination (R^2) values ranging from 0.81 to 0.98. This research represents the first comprehensive investigation into the turbulent flame characteristics of premixed ethane/air and ethane/hydrogen/air mixtures, providing valuable insights into the behaviour of turbulent premixed flames.

2. Experimental set-up and methodology

The experimental measurements were conducted using a Leeds MK-II combustion vessel, which is a spherical, fan-stirred, constant-volume device made of stainless steel with a diameter of 380 mm. The schematic of Leeds Fan-Stirred combustion vessel and the high-speed Schlieren imaging system is shown in Fig. 1. The Leeds MK-II combustion vessel features two pairs of 150 mm diameter orthogonal windows, positioned to enable visualization of flame propagation in the central region. Two 2 kW internal coiled electric heaters which mounted inside the vessel wall were equipped to heat the vessel and mixtures to 360 K. The combustion vessel was equipped with four identical, eight-bladed fans which were arranged in a tetrahedron configuration to optimize homogenous isotropic turbulence. Each individual fan is equipped with eight blades, each approximately 75 mm in length, and the distance between the edges of each blade is roughly 72 mm. Each fan is driven by an 8-kW electric motor, and a motor is controlled by a solid-state variable frequency converter with a speed control range of 200–10000 rpm.

The turbulent flow within the combustion vessel was quantified using particle image velocimetry (PIV) across a range of conditions: fan rotation speeds from 1000 to 6000 rpm, temperature between 300 K to 400 K, and pressure from 0.1 to 1 MPa [40]. The root-mean-square turbulent velocity (u') along with the integral length scale (l) were found insensitive to variations in pressure and temperature in the unburned flow. It was observed that u' within the vessel increases linearly with the fan's rotational speed (rpm), f, expressed as:

$$u' = 0.00124f. \tag{1}$$

Under the current experimental conditions, the integral length scale exhibited a marked insensitivity to variations in fan speeds, consistently maintaining a value in the vicinity of 2 cm.

The experimental conditions in current study are detailed in Table 1. The combustible ethane/hydrogen ($X_{H_2} = 0$ %, 25 %, 50 %, 75 % and 100 % hydrogen by volume) mixtures were prepared quantitively in the combustion vessel with concentrations based on the partial pressure method. The purities of ethane and hydrogen were 99.9 % and 99.95 % respectively. The volumetric percentage of hydrogen X_{H_2} in the ethane/hydrogen/air mixtures was calculated using the formula: $X_{H_2} = V_{H_2}/(V_{H_2} + V_{C_2H_6})$, where V_{H_2} and $V_{C_2H_6}$ represent the volume fractions of hydrogen and ethane in the fuel blends, respectively. The total equivalence ratio ϕ is calculated as:

Table 1
Experimental conditions in current measurements.

Mixture	Equivalence ratio	u'(m/s)	Temperature (K)	Pressure (MPa)
$X_{H_2} = 0$ %	0.8, 0.9, 1, 1.1, 1.2	1, 3, 5	300, 360	0.1 and 0.5
$X_{H_2} = 25$ %	0.8, 0.9, 1, 1.1, 1.2	1, 3, 5	300	0.1
$X_{H_2} = 50$ %	0.8, 0.9, 1, 1.1, 1.2	1, 3, 5	300	0.1
$X_{H_2} = 75$ %	0.8, 0.9, 1, 1.1, 1.2	1, 3, 5	300	0.1
$X_{H_2} = 100$ %	0.8, 0.9, 1, 1.1, 1.2	1, 3, 5	300	0.1

$$\phi = \frac{F/A}{(F/A)_{st}} \tag{2}$$

Where (F/A) is the total fuel to air ratio and $(F/A)_{st}$ is the stochiometric value of fuel to air ratio. The stoichiometric combustion formula for ethane/ hydrogen/air mixtures is expressed as:

$$(1 - X_{H_2})C_2H_6 + X_{H_2}H_2 + \left(\frac{3.5}{\phi}(1 - X_{H_2}) + \frac{X_{H_2}}{2\phi}\right)(O_2 + 3.76N_2) \tag{3}$$

Prior to each mixture preparation, the combustion vessel undergoes a vacuuming process to achieve an absolute pressure of less than 10 mbar. Subsequently, it is filled with dry compressed air to an absolute pressure of 2 bars. This procedure is repeated twice to ensure the removal of any residual substances.

The mixture was ignited within the vessel through a centrally located spark plug with minimum ignition energies of about 1 mJ. Four fans are continuously operated before and during the ignition process to homogeneously mix the mixtures and generate turbulent conditions. The pressure during the combustion process was measured by a Kistler 701A dynamic pressure transducer which flushed to the inner wall of the vessel. The output charge from this transducer was converted by a Kistler 5007 charge amplifier, which was sampled at 50 kHz. For each set of experimental conditions, three experiments were conducted. In all experimental results, the average values are represented along with standard deviation error bars plotted around the mean values.

The turbulent flame propagation images were captured by high-speed Schlieren imaging system. The Schlieren imaging setup included a 150-watt adjustable tungsten lamp, two plano-convex lenses, and a high-speed digital camera (SpeedSense 2640, DANTEC DYNAMICS Co., Ltd, UK). The camera was operated at speeds of 10,000 frames/s for $u' =$

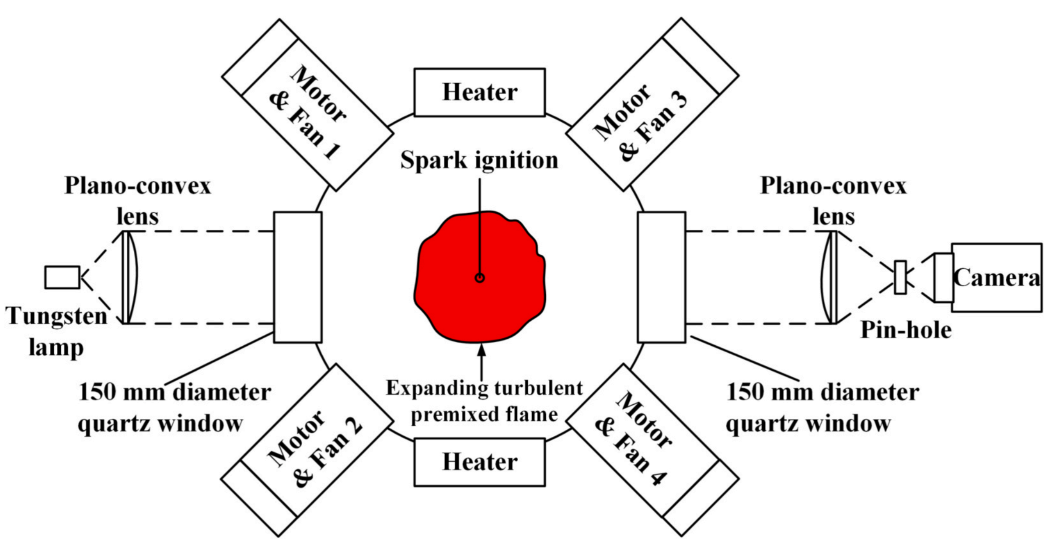

Fig. 1. Schematic of the Leeds fan-stirred combustion vessel and high-speed Schlieren imaging system.

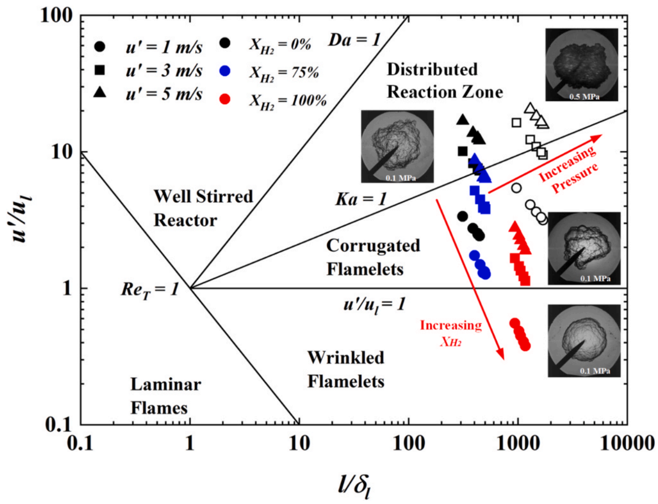

Fig. 2. Partial experimental conditions on Peters-Borghi [45] diagram. Open symbols represent 0.5 MPa, and solid symbols represent 0.1 MPa.

1 m/s, 20,000 frames/s for $u' = 3$ m/s, and 30,000 frames/s for $u' = 5$ m/s. This setup offered a resolution of 512 × 512 pixels with a pixel size of 0.265 mm per pixel. For analysis, all Schlieren images of flame propagation were post-processed using MATLAB [41], employing the 'binarizing-thresholding' technique for image processing. Each post-processed image was meticulously compared with its corresponding raw image to ensure that all burned areas were accurately detected. The Schlieren images were binarized to calculate the 2D projection burned area of the 3D flame front, A. The equivalent flame radius, r_{sch}, is defined as $r_{sch} = \sqrt{A/\pi}$. Consequently, the instantaneous turbulent flame speed, with respect to the burnt side, is calculated as $S_{sch} = dr_{sch}/dt$.

The research conducted by Bradley et al. [42] reported that the definition of TBV is contingent upon the specific flame radius selected for analysis. In their study, Mie scattering and schlieren imaging techniques were utilized to examine the distribution and surface properties of turbulent premixed flames. Their study demonstrated that under isotropic conditions within the structured field, at any given radius, a volumetric reference radius r_v which defined as the total volume of unburned gas within the flame sphere is equal to the total volume of burned gas outside this region. At r_v, the TBV matches the product of the flame speed and the burned to unburned density ratio ρ_b/ρ_u. Bradley et al. [40] further compared the volumetric reference radius (r_v), determined from Mie scattering, with the corresponding Schlieren-based radius (r_{sch}) across a series of experiments. This comparison revealed an average optimal linear relationship between r_v and r_{sch}. Based on Schlieren imaging measurements, the volumetric turbulent burning velocity, u_{tr} can be expressed as:

$$u_{tr} = 1/1.11(\rho_b/\rho_u)(dr_{sch}/dt) \quad (4)$$

Eq. (4) has been widely adopted in prior studies [23,25,28,43,44] for determining the TBV in various fuel/air mixtures and is employed in the present work for the same purpose. The fundamental parameters, including the laminar burning velocity u_l used in the present study were obtained from the measurements reported in [11]. The laminar flame thickness is calculated using the expression:

$$\delta_l = \frac{v}{u_l Pr} \quad (5)$$

where v is the kinematic viscosity and P_r is the Prandtl number, defined as $P_r = \frac{v}{\alpha}$ with α representing the thermal diffusivity.

3. Results and discussion

3.1. Turbulent combustion regimes

The Peters-Borghi diagram is employed in the present study to classify the combustion regimes, as shown in Fig. 2, accompanied by corresponding Schlieren images for visual reference. The turbulent conditions investigated span multiple regimes, including wrinkled flamelets, corrugated flamelets, and the distributed reaction zone. For pure ethane/air flames, increasing u' from 1 m/s to 5 m/s leads to a transition from the corrugated flamelets regime to the distributed reaction zone, where the Karlovitz number (Ka) exceeds unity. In this regime, flame stretch becomes significant, and the smallest turbulent eddies begin to penetrate the preheat zone, resulting in an increased flame surface area due to enhanced wrinkling [45]. In contrast, at fixed u', increasing X_{H_2} raises u_l, and reduces δ_l, thereby decreasing the ratio u'/u_l, increasing l/δ_l, and shifting the flame regime toward the bottom right side of the diagram. For ethane/air mixtures, an increase in pressure reduces the δ_l and u_l, which increases both l/δ_l and u'/u_l ratio, resulting in a shift toward the upper right region of the diagram.

3.2. Turbulent flame morphologies

The morphological variations of both turbulent and laminar flames under different X_{H_2}, pressure and u' at a $r_{sch} = 40$ mm are depicted in Fig. 3. An increase in temperature does not produce significant changes in flame morphology. The images are arranged from bottom to top to reflect the transition from laminar to increasingly turbulent flames as u' rises. Images (m) and (n) in Fig. 3 illustrate how increasing pressure alters the flame surface, transitioning from a smooth to a cellular structure. This transformation, resulting from reduced flame thickness, intensifies hydrodynamic instability due to pronounced density gradients across the flame front. Furthermore, the progression from smooth to increasingly cracked flame surfaces, as shown in images (n), (o), and (p) in Fig. 3, corresponds with rising levels of X_{H_2}. Such a transition is linked to a decrease in the Lewis number, amplifying the effects of thermal-diffusivity (TD) instability.

For the pure ethane/air flames increasing u' from 0 to 5 m/s, as shown in Fig. 3 from images (n) to (b), leads to progressively greater flame surface wrinkling, deformation, and finer-scale structures. This change is attributed to the decreasing Kolmogorov length scale, η as increase in u'. Notably, at $u' = 5$ m/s, the pure ethane/air flames at both 0.1 MPa (Fig. 3 (b)) and 0.5 MPa (Fig. 3 (a)) exhibit highly distorted shapes, deviating significantly from spherical fronts. According to Fig. 2, both cases fall within the distributed reaction zone where Ka greater than unity. In this regime, the eddy lifetime is shorter than the chemical reaction time, indicating that the reaction cannot be completed within the lifetime of the smallest eddies. Consequently, turbulent eddies can penetrate the preheating zone of flamelets, thicken the zone, and enhance heat and mass transfer within it [46].

The effect of hydrogen addition (X_{H_2}) is illustrated in Fig. 3 (b)-(d), where the flame structure at $u' = 5$ m/s gradually transitions from a highly deformed to a more spherical shape. This demonstrates that increasing X_{H_2} enhances flame stability and reduces flame front wrinkling. This stabilizing effect is attributed to the increase in u_l, which shortens the chemical time scale (δ_l/u_l), thereby reducing the Karlovitz number. As shown in Fig. 2, this shift corresponds to a transition from the distributed reaction zone to the corrugated flamelets regime. The addition of hydrogen helps stabilize the ethane flame by accelerating the burning rate and reducing the local chemical timescale.

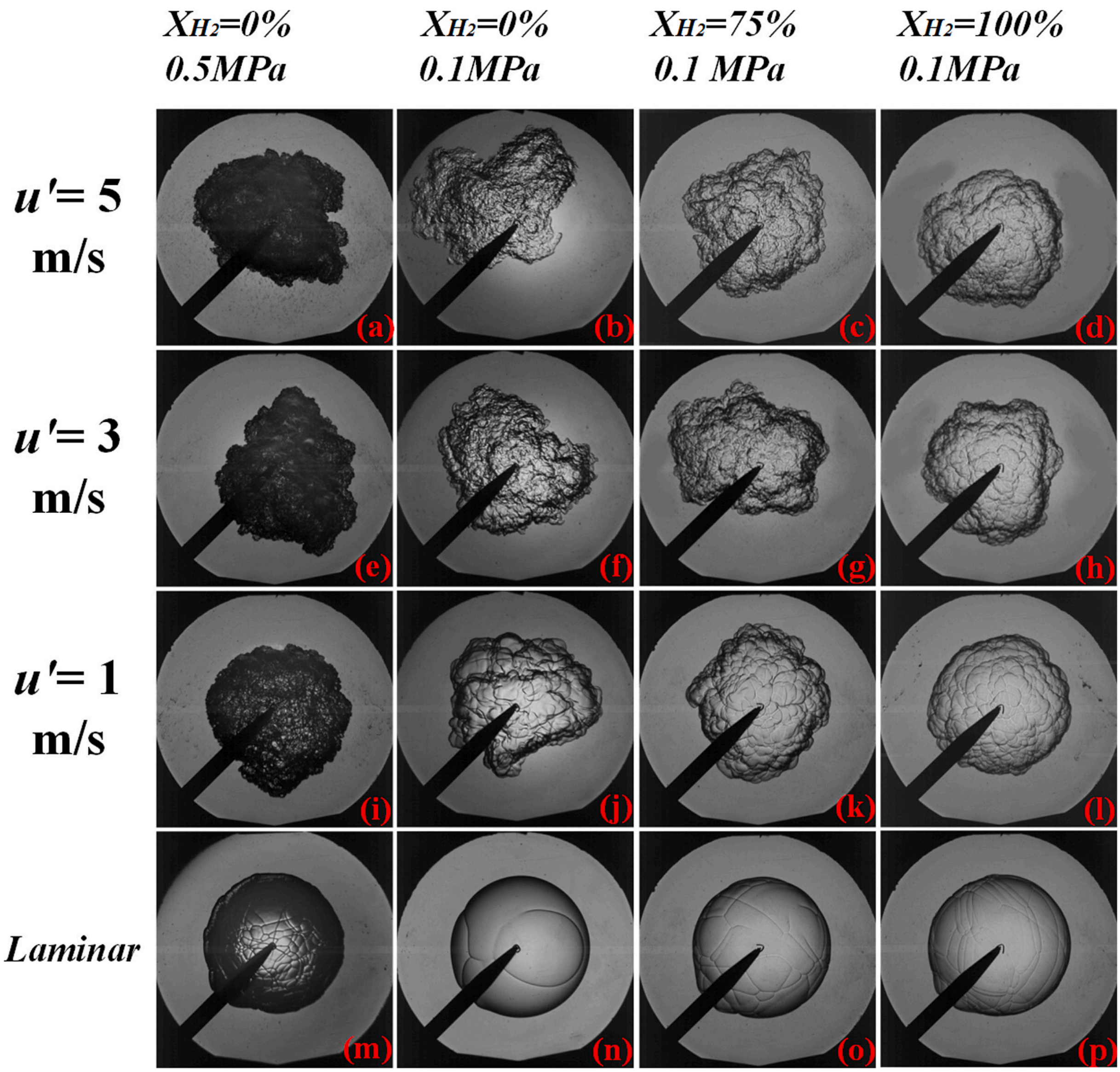

Fig. 3. Laminar and turbulent flame morphologies at $r_{sch} = 40$ mm for different X_{H_2}, pressure and u' for stoichiometric mixtures.

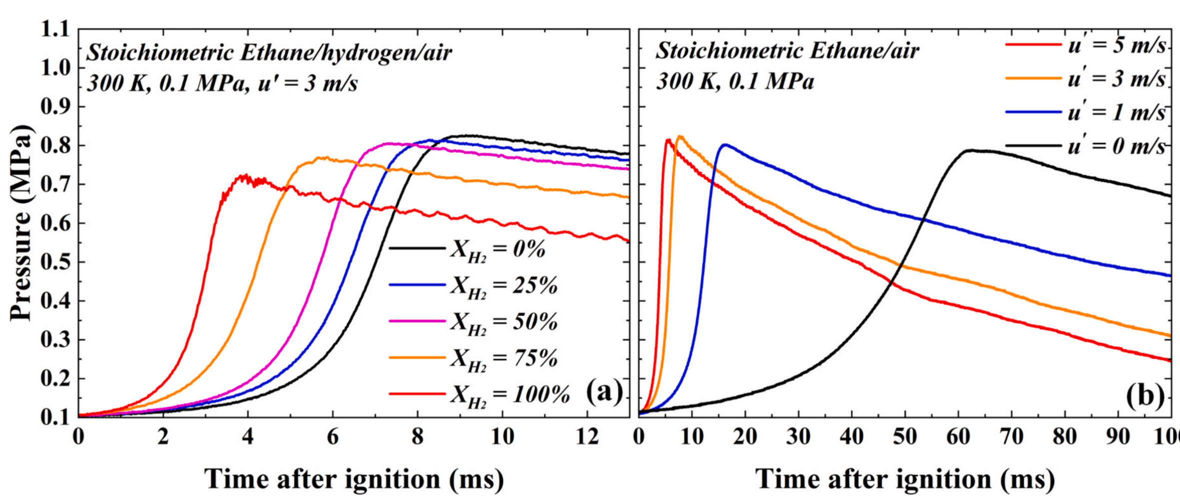

Fig. 4. Impact of u' (a) and hydrogen additions (b) on the pressure evolution of stoichiometric ethane/hydrogen/air mixtures at condition of 300 K, 0.1 MPa.

3.3. Turbulent pressure evolution

The evolution of pressure throughout the combustion process has been illustrated in Fig. 4. As shown in Fig. 4 (a), the evolutions of the pressure are strongly affected by u'. As u' increases, the time interval from the start of ignition to the peak pressure correspondingly decreases. This observation suggests that an increase in u' significantly enhances the burning rate. A similar trend was observed in [24] for hydrogen turbulent flame. Despite the variation of u', the maximum pressures at the end of combustion consistently reach 0.8 MPa across all levels of u'. Additionally, Fig. 4 (b) reveals that at a given$u' = 3$ m/s, an increase in X_{H_2} leads to a further decrease in the time from ignition onset to maximum pressure. This trend underscores the role of hydrogen addition in promoting the burning velocity, due to its positive influence on overall thermal and chemical kinetics [47].

3.4. Turbulent flame speed

The evolutions of the flame radius over time are depicted in Fig. 5(a), (c) and (e), showing the effects of u' and X_{H_2} on flame development. Overall, increasing u' and X_{H_2} promotes the growth of the flame radius, indicating that both enhanced turbulence and higher hydrogen content facilitate faster flame propagation. Fig. 5(b), (d) and (f) present the corresponding turbulent flame propagation speeds (S_{sch}) plotted against flame radius, with each curve representing the average of three experiments. As observed in Fig. 5(b) and (d), at both 0.1 MPa and 0.5 MPa pressures, S_{sch} increases significantly with increasing u'. Moreover, at a fixed u', S_{sch} continues to rise as the flame expands. This behavior is consistent with previous observations for turbulent expanding hydrogen/air flames [24] and ammonia/hydrogen/air flames [31]. Zhang et al. [48] demonstrated that the sphericity of the turbulent flame front decreases with flame growth, reflecting a progressive increase in flame surface wrinkling.

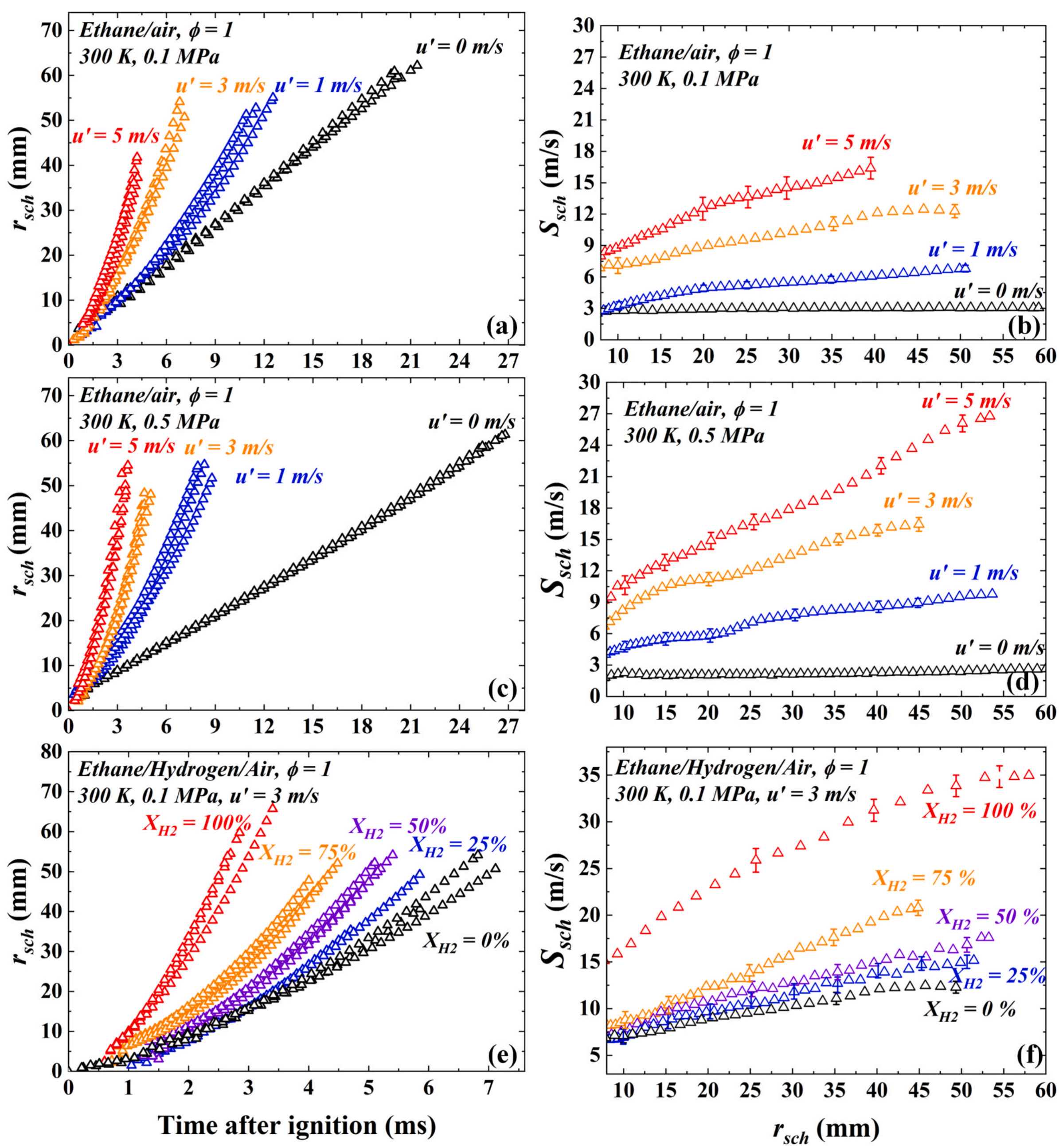

Fig. 5. Variation of flame radius over time in (a), (c), and (e); variation of flame propagation speed with flame radius in (b), (d), and (f).

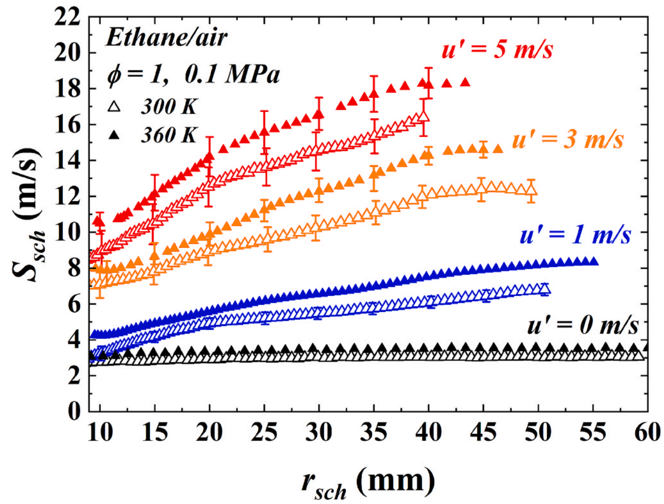

Fig. 6. Variation of flame propagation speed with flame radius, highlighting the effect of initial temperature. Open symbols represent 300 K, while solid symbols represent 360 K.

Fundamentally, Abdel-Gayed et al. [22] and Bradley et al. [49] attributed turbulent flame acceleration primarily to increased flame front wrinkling induced by turbulence. As the flame radius grows, the flame interacts with a larger number of turbulent eddies, which enhances surface wrinkling and promotes faster flame propagation. Comparing the turbulent flame propagation speeds in Fig. 5. (b)&(d), it is noted that an increase in pressure at a constant u' results in a higher turbulent flame propagation speed. As shown in Fig. 5. (f), an increase in X_{H_2} at a fixed $u' = 3$ m/s also results in a noticeable increase in flame propagation speed. This enhancement can be attributed to both thermal and chemical effects associated with hydrogen addition, including a rise in adiabatic flame temperature and increased production of reactive species such as H, O, and OH radicals [11]. The temperature dependence of S_{sch} with flame radius for different u' values is presented in Fig. 6. Under all u' conditions, increasing the initial temperature from 300 K to 360 K results in a clear increase in S_{sch}, due to the thermal enhancement of reaction rates.

To separate the effects of laminar flame propagation on turbulent flame propagation, the turbulent flame speed is normalized by the corresponding unstretched laminar flame speed, S_s, and the results are plotted in Fig. 7. Fig. 7(a) illustrates the effect of pressure on the normalized turbulent flame speed, $\frac{S_{sch}}{S_s}$, under different u' conditions. Increasing the pressure from 0.1 to 0.5 MPa significantly raises the normalized $\frac{S_{sch}}{S_s}$ across all u' conditions, indicating that higher pressure enhances the turbulent acceleration of flame propagation. This trend is consistent with previous findings for turbulent ammonia/oxygen/nitrogen flames [26].

Several studies have elucidated the effects of pressure on turbulent flame propagation speed. The study by Wang et al. [32] reported that increasing pressure enhances flame curvature and reduces the thickness of laminar flamelets, which promotes more pronounced flame surface wrinkling at progressively smaller scales. Another potential mechanism is the amplification of cellular flame instability with increasing pressure, which leads to the formation of fine-scale cellular structures that accelerate flame propagation. Turbulent wrinkling may further amplify this hydrodynamic instability. This mechanism is supported by the

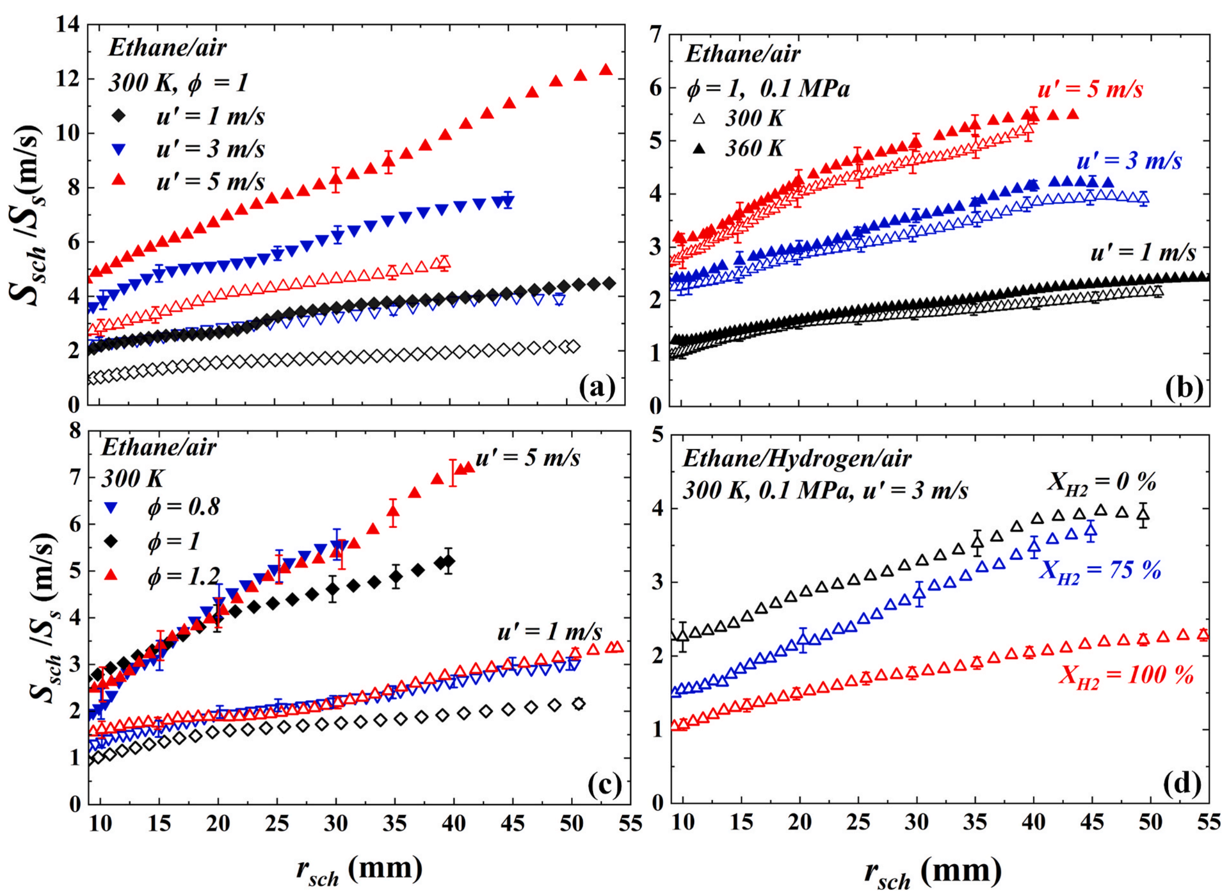

Fig. 7. Normalized turbulent flame speed, $\frac{S_{sch}}{S_s}$ against flame radius. (a) Solid symbols represent 0.5 MPa, and open symbols represent 0.1 MPa. (b) Solid symbols represent 360 K, and open symbols represent 300 K. (c) Solid symbols indicate $u' = 5$ m/s and open symbols indicate $u' = 1$ m/s.

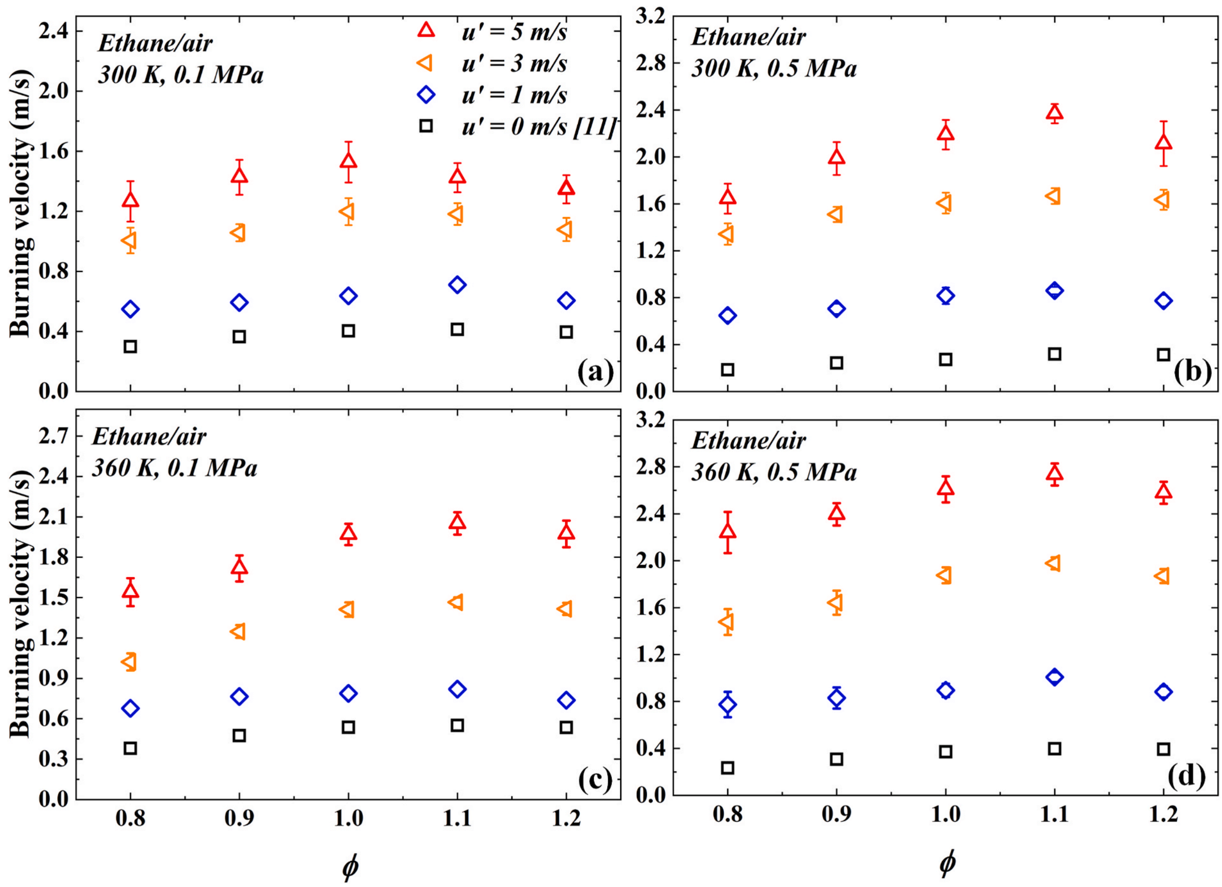

Fig. 8. The turbulent burning velocity, $u_{tr(30mm)}$ and laminar burning velocity of ethane/air under various conditions.

numerical study by Creta and Matalon [50], which demonstrates that upon the onset of hydrodynamic instability, corrugated structures replace the planar conformation of the flame, thereby enhancing its resilience to turbulence. Their findings corroborate the hypothesis that the coupling of hydrodynamic instability with turbulence intensifies flame surface corrugation, thereby increasing the propagation speed. Furthermore, direct numerical simulations (DNS) by Howarth et al. [51] showed that turbulence and cellular instability elicit similar responses in premixed flames. Turbulence can couple with cellular instability, further enhancing the wrinkling of the turbulent flame front.

Subplot (b) and (c) in Fig. 7 show the effects of temperature and equivalence ratio on the normalized $\frac{S_{sch}}{S_s}$ under different u' conditions. As shown in Fig. 7(b), increasing the temperature from 300 K to 360 K leads to a consistent rise in $\frac{S_{sch}}{S_s}$ across all u'. This trend suggests that at elevated temperatures, the relative enhancement of flame propagation due to turbulence becomes more pronounced. Subplot (c) in Fig. 7 demonstrates that, compared to stoichiometric mixtures, rich or lean conditions result in higher $\frac{S_{sch}}{S_s}$. A similar trend has been reported by Lawes et al. [23] for other hydrocarbon fuels such as methane, methanol, and *iso*-octane. The effect of hydrogen addition (X_{H_2}) on the normalized $\frac{S_{sch}}{S_s}$ is shown in subplot (d). The $\frac{S_{sch}}{S_s}$ decreases with increasing X_{H_2} across all flame radii. At$r_{sch} = 45$ mm, the turbulent flame speed for pure ethane reaches four times the laminar flame speed, whereas for pure hydrogen, it is only about twice. This suggests that while hydrogen addition to ethane increases laminar flame speed, it reduces the relative enhancement induced by turbulence.

3.5. Turbulent burning velocity

As demonstrated in Figs. 6 and 7, the turbulent flame propagation speed increases nonlinearly with the flame radius. Due to this nonlinear behaviour, direct comparison between cases becomes less straightforward. To quantitatively compare the propagation characteristics of turbulent flames, it is convenient to select a reference radius to define the TBV. In this study, for each experiment, a schlieren flame radius of 30 mm is selected as the reference radius for defining the TBV, $u_{tr(30mm)}$. Selecting this radius is supported by several factors. According to the studies by Chen et al. [52] and Burke et al. [53], a flame radius of 30 mm is sufficiently large to ensure no residual effects from the spark plug energy and is free from the effects of chamber confinement. This selection is particularly relevant under high turbulence conditions ($u' = 5$ m/s), where the turbulent flame tends to move away from the center of the optical window. Consequently, only flame radii less than 30 mm are sometimes measurable before parts of the flame kernel perimeter become invisible. Moreover, the 30 mm reference turbulent flame radius is widely used in studies involving hydrogen [25], methane[23,28], *iso*-octane [23], methanol [43], and thermally cracked hydrocarbon fuel [54]. Using this reference radius facilitates comparison of TBV across these different fuels.

Fig. 8 presents $u_{tr(30mm)}$ as defined in Eq. (4) at the reference radius of 30 mm, under$u' = 1$, 3 and 5 m/s, along with u_l derived from [11]. These images encompass a range of experimental conditions, covering temperatures from 300 to 360 K, pressures from 0.1 to 0.5 MPa, and equivalence ratios from 0.8 to 1.2. For most conditions, the maximum u_{tr} is observed with $\phi = 1.1$. The highest u_{tr} within the scope of this study for ethane/air mixtures is recorded at 2.8 m/s under conditions of 360 K, 0.5 MPa, and $u' = 5$ m/s. Overall, the variable u' has a substantial impact on the magnitude of u_{tr}. Increases in both temperature and pressure contribute to a rise in u_{tr}. This phenomenon is primarily due to higher temperatures enhancing the reactivity of the mixture, thereby increasing the burning velocity.

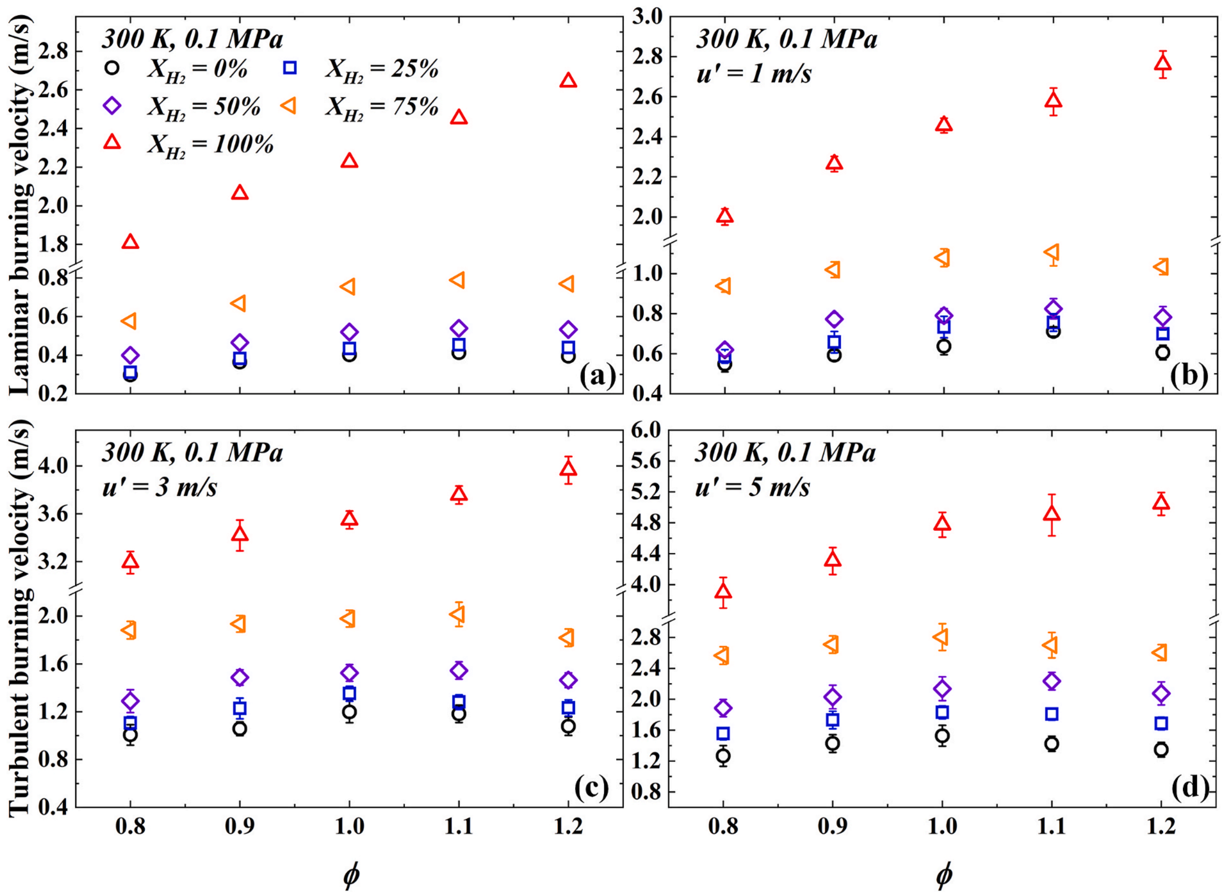

Fig. 9. The turbulent burning velocity, $u_{tr(30mm)}$ and laminar burning velocity of ethane/hydrogen/air under various conditions.

The effects of increasing X_{H_2} on u_l and $u_{tr(30mm)}$, at u' values of 1, 3 and 5 m/s, are illustrated in Fig. 9, specifically in (a), (b), (c) and (d) respectively. For all u' values, both u_l and u_{tr} increases with X_{H_2}. This increase is attributed to the enhancement of chemical kinetics and thermal effects that accompany the rise in X_{H_2}. The range of burning velocities varies from a minimum of 0.3 m/s for laminar ethane/air mixtures at $\phi = 0.8$ to a maximum of 5 m/s for turbulent hydrogen/air mixtures at $\phi = 1.2$ and$u' = 5$ m/s. For all fuel mixtures, u_l and u_{tr} generally increase with equivalence ratio from $\phi = 0.8$ to $\phi = 1$ or 1.1, followed by a decrease at $\phi = 1.2$. In contrast, hydrogen/air mixtures exhibit a continuous increase in both u_l and u_{tr} over the entire range from $\phi = 0.8$ to 1.2.

3.6. The effects of u_k'/u' onu_{tr}

The earlier study by Abdel-Gayed et al. [22] observed that the turbulent flame propagation speed continuously increases with flame radius. This behavior was attributed to the growing flame radius interacting with a larger volume of turbulent eddies, thereby increasing the overall turbulent energy available to wrinkle the flame front. Subsequently, Bradley et al. [49] introduced the ratio $\frac{u_k'}{u'}$, where u_k' is the effective root-mean-square turbulent velocity contributing to flame front wrinkling, and u' is the overall root-mean-square turbulent velocity. This ratio was proposed to represent the fraction of turbulent energy that effectively contributes to the wrinkling of the flame surface. A unity value of this ratio indicated that the whole turbulence energy contributes to the wrinkling of flame. According to [49], the ratio of u_k'/u' is mathematically expressed as:

$$u_k'/u' = \left[\frac{\sqrt{15}}{R_\lambda}\int_{\bar{k}_{\eta k}}^{\bar{k}_{\eta G}} \bar{S}(\bar{k}_\eta)d\bar{k}_\eta\right]^{0.5} \tag{6}$$

Here, $\bar{S}(\bar{k}_\eta)$ is the dimensionless power spectral density, expressed in terms of a dimensionless wavenumber $\bar{k}_\eta$,:

$$\bar{S}(\bar{k}_\eta) = \frac{0.01668R_\lambda^{2.5} + 3.74R_\lambda^{0.9} - 70R_\lambda^{-0.1}}{1 + (0.127R_\lambda^{1.5}\bar{k}_\eta)^{5/3} + (1.15R_\lambda^{0.622}\bar{k}_\eta)^4 + (1.27R_\lambda^{0.357}\bar{k}_\eta)^7} \tag{7}$$

In this expression, R_λ is the Reynolds number expressed as $u'\lambda/\nu$, with Taylor scale, λ, and kinematic viscosity, ν. The dimensionless wavenumber $\bar{k}_\eta$, which is derived from the wavenumber multiplied by the Kolmogorov length scale, η. The upper limit, $\bar{k}_{\eta G} = \frac{2\pi\eta}{l_G}$ is determined by the size of the smallest eddy that can be chemically reacted, the Gibson scale, l_G. Whereas the lower limit $\bar{k}_{\eta k} = \frac{2\pi\eta}{nL}$ signifies the maximum wavelength, nL typically close to the diameter of the flame. Here the n is the flame diameter normalized by the integral length scale, l.

Fig. 10 (a), (c) and (e) illustrate the u_k'/u' ratio against r_{sch} for stoichiometric ethane/hydrogen/air mixtures under varying initial pressures, X_{H_2} and u' values. For all conditions, the development of the flame radius correlates with an increasing of u_k'/u' ratio. As the turbulent flame propagates, the increasing flame radius leads to a decrease in $\bar{k}_\eta$. According to Eq. (7), this results in an increase in $\bar{S}(\bar{k}_\eta)$, further increasing the integration term in Eq. (6) and the ratio of u_k'/u'. This indicates an increasing amount of turbulent energy spectrum wrinkling the flame front. At the $r_{sch} = 30$ mm, the $u_k'{}_{(30mm)}/u'$ ratio is approximately 0.7 suggesting that around 70 % of the turbulent energy spectrum contributes to the wrinkling of the flame front. In the current experimental setup, it is not possible to achieve a condition where u_k'

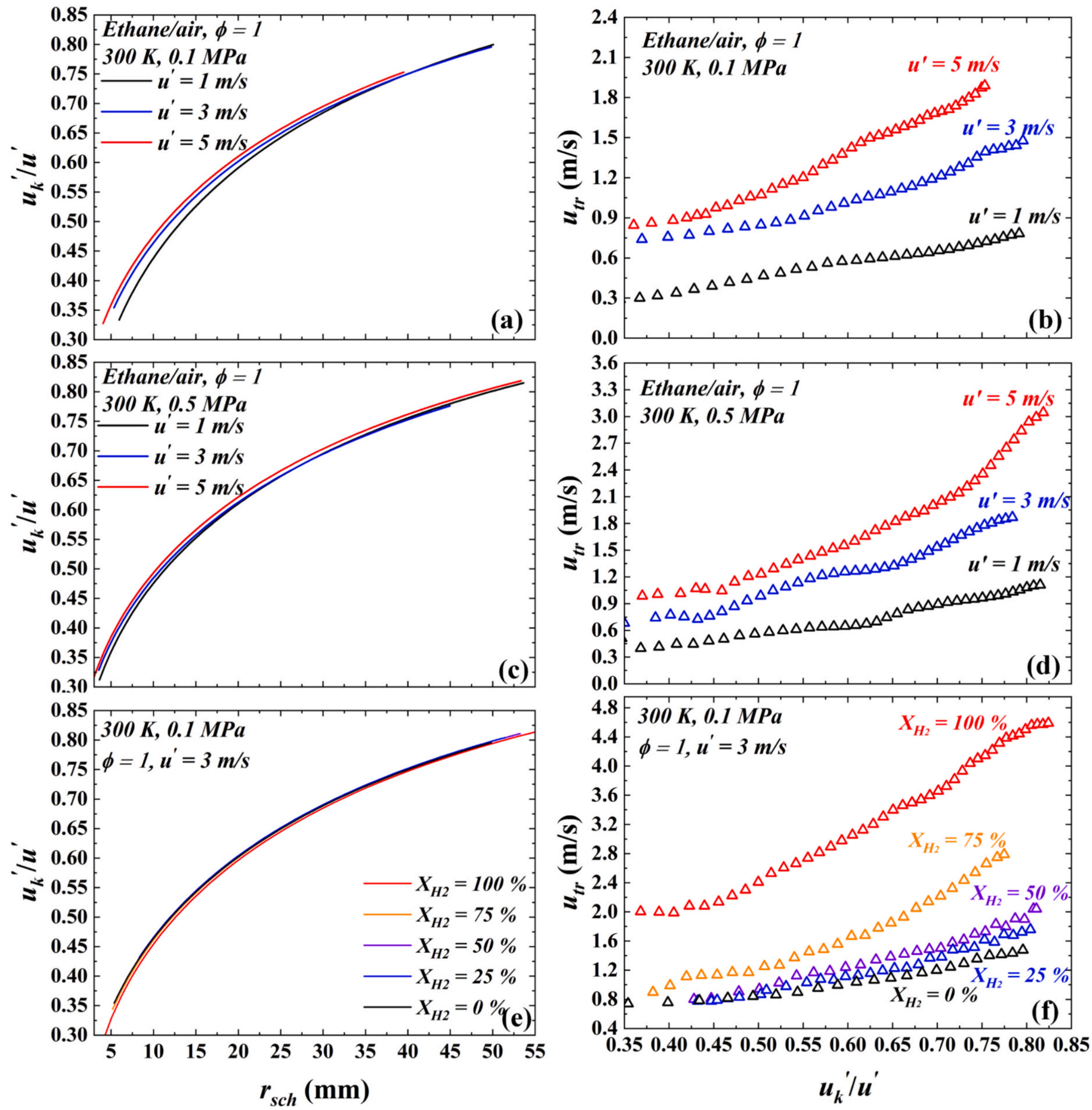

Fig. 10. Variations of u_k'/u' against r_{sch} in (a), (c) and (e), and u_{tr} with u_k'/u' in (b), (d) and (f).

equals u'. This is demonstrated as r_{sch} reaches 50 mm, which is close to the maximum visualization radius through the optical window, with the u_k'/u' ratio reaching around 0.82. The relationship between u_{tr} and the ratio u_k'/u' is shown in Fig. 8 (b), (d) and (f). Under all conditions, an increase in the u_k'/u' ratio leads to an increase in u_{tr}, further demonstrating that an increasing amount of turbulent energy spectrum accelerating the turbulent burning velocity.

3.7. Turbulent burning velocity correlations

Given that TBV is a crucial input parameter in turbulent combustion modelling and simulations, numerous studies [35,36,39,55] have focused on establishing a unified correlation for TBV based on experimental data. The comprehensive and general among these is the *U-K* diagram correlation proposed by Bradley et al. [38,39]. In the present study, the current measurements, along with ethanol data from Ref. [38], are correlating using the same *U-K* framework. This correlation employs two dimensionless parameters: *U*, and the Karlovitz stretch factor, *K*, and is expressed as:

$$U = \frac{u_{tr(30mm)}}{u_{k'(30mm)}} = \alpha K^{\beta}, \text{ for } (0.002 < K < 1.8) \tag{8}$$

Here, $u_{tr(30mm)}$ is the turbulent burning velocity at$r_{sch} = 30$ mm and the effective root-mean-square turbulent velocity at this radius is estimated as $u_{k'(30mm)} = 0.7\ u'$. The parameter K represents the ratio of turbulent strain rate ($\frac{u'}{\lambda}$) to a laminar flame strain rate ($\frac{u_l}{\delta_l}$), and is formulated as follows:

$$K = (\frac{u'}{\lambda})/(\frac{u_l}{\delta_l}) \tag{9}$$

The Taylor microscale, λ, can be estimated as [56]:

$$\lambda = 4\left(u'^{-0.5} L^{0.5} \nu^{0.5}\right) \tag{10}$$

In the original *U-K* diagram formulation, the constants α and β are related to the strain rate Markstein number, Ma_{sr}, which is introduced to account for the effects of strain rate on TBV. This incorporation is based on findings from previous studies [50,57], which highlight the

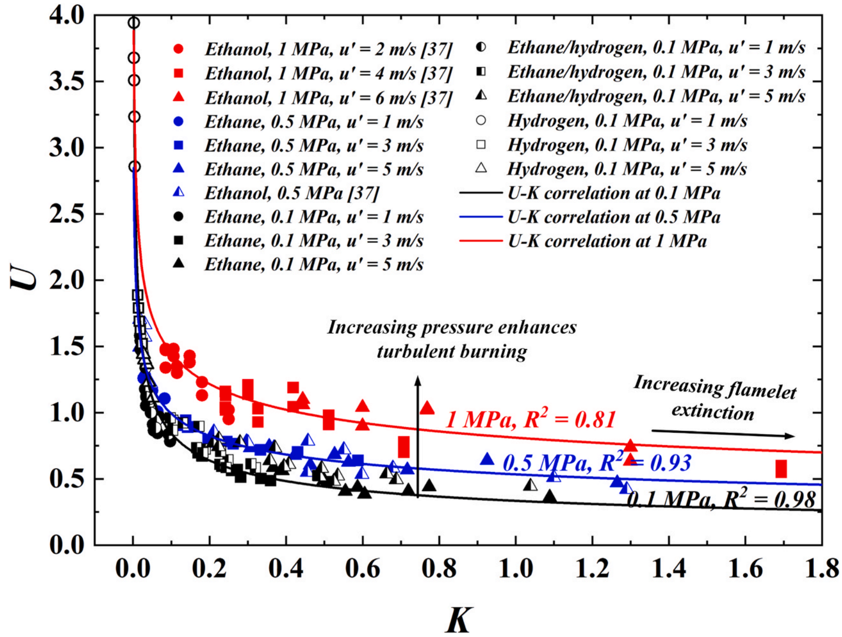

Fig. 11. Correlation of U with K across various pressures under current experimental conditions and from [38] in 1 MPa.

Table 2
Constants α and β for Eq. (8) at different pressures.

	0.1 MPa	0.5 MPa	1.0 MPa
α	0.335	0.534	0.790
β	−0.402	−0.269	−0.250

significance of strain rate in augmenting flame surface area, with straining being more influential than curvature in this aspect. However, in practical scenarios, accurately measuring Ma_{sr} has proven challenging, often requiring extensive experimental or numerical analysis. Prior experimental measures of Ma_{sr} have shown considerable variability and large error margins. This inconsistency has led to correlations with a relatively low coefficient of determination, R^2, ranging between 0.66 and 0.88 [38]. These limitations highlight the need and opportunity to simplify and improve the correlation framework to better align with experimental observations.

All current measurements for ethane/air, ethane/hydrogen/air, hydrogen/air, and ethanol/air from [38] are consolidated in Fig. 11. The figure clearly shows that increasing pressure separates the measured data into distinct clusters, indicating that pressure has a significant influence on the correlation between U and K. This observation suggests that a separate correlation should be established for each pressure level to accurately capture the experimental trends. Accordingly, in Fig. 10, three solid curves are plotted using Equation (8) with the fitted constants listed in Table 2. These correlations yield R^2 values of 0.98, 0.93, and

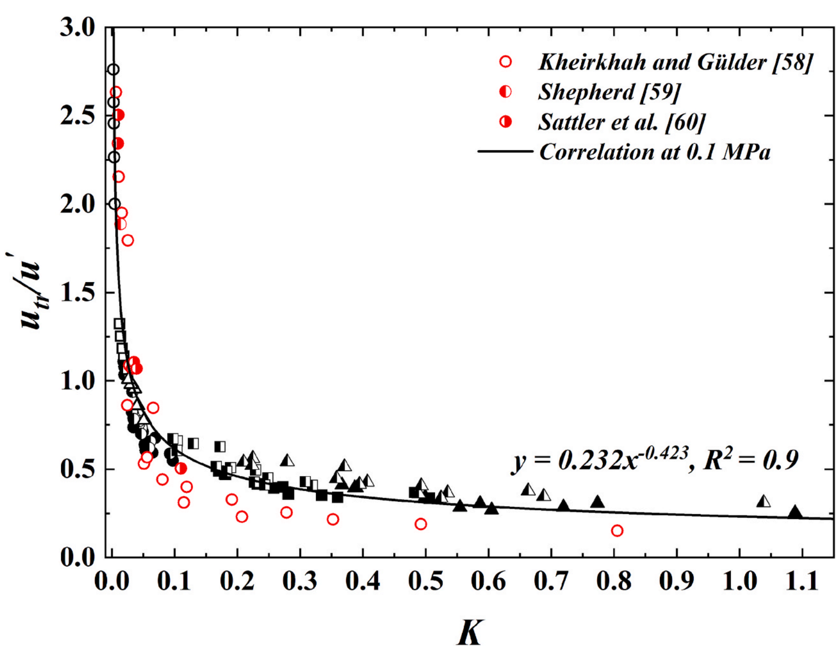

Fig. 12. Correlation of $\frac{u_{tr}}{u'}$ with K based on current measurements using the spherical flame method, along with methane/air data from V-shaped burner experiments reported in Refs. [58–60].

0.81 at 0.1, 0.5, and 1.0 MPa, respectively. The correlations are validated against experimental data within the range $0.002 < K < 1.8$. The constants α and β in Eq. (8) were optimized to best fit the experimental data at each pressure level, and their values are summarized in Table 2.

Previous studies in [39] have classified the *U-K* correlation into three regimes based on the value of *K*: the mild turbulence regime ($K < 0.1$), fully turbulent regime ($0.1 < K < 2$) and a possible flame extinction regime ($K > 2$). However, at very low values of *K*, the parameter *U* becomes less meaningful, as $u' \to 0$, $U \to \infty$, which falls within the scope of laminar conditions. Within the mild turbulence regime, a sharp decrease in *U* with increasing *K* is observed across all pressure levels. In the fully turbulent regime, u' increase further, leading to higher *K* values, while the rate of decrease in *U* becomes more gradual. This behaviour reflects reduced eddy lifetimes and enhanced flame wrinkling. Most of the cases in the present study fall within this regime. At a fixed *K*, increasing in the initial pressure leads to a higher *U*, which can be attributed to pressure-induced enhancement of the turbulent burning velocity. Although further increase in u', pushing *K* beyond 2, may result in flame quenching, no extinction was observed in the present study as *K* approached 1.7.

In addition to spherical flame methods conducted in constant volume combustion vessels, the turbulent burning velocity can also be measured using V-shaped burner experiments, as reported in Refs. [58–60]. To evaluate the consistency of the proposed correlation, the present spherical flame data are compared with these earlier V-shaped flame measurements. Specifically, the current ethane/hydrogen/air flame data at 0.1 MPa from Fig. 11 are re-plotted in Fig. 12 in the form of u_{tr}/u' versus *K*, to match the format used in Refs. [58–60] for methane/air mixtures, also at 0.1 MPa. Overall, the V-shaped burner data show good agreement with the present measurements, following a similar decreasing trend of u_{tr}/u' with increasing of *K*, though slight deviations are observed. In the very mild turbulence regime ($K < 0.05$), the data from V-shaped burner align closely with the present data. However, for $K > 0.05$, the V-shaped burner data tend to lie below the spherical flame data, despite exhibiting a comparable dependence on *K*.

This discrepancy may be attributed to differences in the definition of the reference location for turbulent burning velocity evaluation. In V-shaped burners, the turbulent burning velocity is typically extracted at the position where the progress variable, $c = 0.5$, representing a half-burned surface. According to Ref. [38], the turbulent burning velocity measured at half burning surface ($r_{0.5}$) is approximately 20 % lower than that obtained from the volumetric flame radius (r_v), which is used in the present spherical flame analysis. This difference in evaluation location likely contributes to the lower values of u_{tr}/u' observed in the V-shaped flame data. A power-law correlation is proposed to represent both the current measurements and the V-shaped flame data at 0.1 MPa, as shown by the black solid line in Fig. 12, yielding a coefficient of determination of R^2 of 0.9. This result indicates that, despite differences in experimental configurations, the dependence of u_{tr}/u' on *K* remains consistent across both methods.

4. Conclusions

To date, no experimental datasets have been available for turbulent premixed ethane/air and ethane/hydrogen/air flames. Addressing this research gap, the present study provides comprehensive measurements of key flame characteristics, including pressure evolution, turbulent flame speed, and turbulent burning velocity, for these mixtures in a fan-stirred combustion vessel over a wide range of operating conditions. The current measurments cover multiple combustion regimes as defined by the Peters-Borghi classification, including wrinkled flamelets, corrugated flamelets, and distributed reaction zones. The hydrogen addition to the ethane was found to increase the laminar burning velocity reduce the chemical time scale and promote regime transitions from distributed to flamelet structures. It also enhances flame stability and broadens the extinction limit. Furthermore, increases in temperature, pressure, hydrogen content, and u' lead to significant increases in both turbulent flame propagation speed and turbulent burning velocity. Notably, increasing hydrogen addition in the ethane/air mixture can weaken the turbulent acceleration effects on the turbulent flame propagation. In contrast, elevated temperature and pressure substantially amplify turbulent acceleration effects.

The *U-K* turbulent burning velocity correlation has been refined by introducing pressure as a key parameter in place of Ma_{sr}. The revised correlation accommodates four different fuel mixtures at pressures up to 1.0 MPa and shows excellent agreement with experimental results, yielding R^2 ranging from 0.81 to 0.98 for both the current data and ethanol/air measurements from Ref. [38]. This represents a significant improvement over the previously reported range of 0.66 to 0.88 in Ref. [38]. A comparison between spherical and V-shaped flame configurations further indicates that, despite differences in experimental setups, the dependence of u_{tr}/u' on *K* remains consistent across both methods.

CRediT authorship contribution statement

Jinzhou Li: Writing – original draft, Visualization, Validation, Methodology, Investigation, Formal analysis. **Junfeng Yang:** Writing – review & editing, Supervision, Resources, Project administration, Methodology, Funding acquisition, Conceptualization.

Declaration of competing interest

The authors declare that they have no known competing financial interests or personal relationships that could have appeared to influence the work reported in this paper.

Acknowledgements

Dr. J. Yang thanks EPSRC (Grant No. EP/W002299/1) for the financial support. Dr. J. Li acknowledges Shell Global Solution Ltd. (UK) provides partial financial support the PhD study. Authors would like to acknowledge the valuable discussions with Prof. Derek Bradley and Dr. Marwaan AL-Khafaji.

Appendix A. Supplementary data

Supplementary data to this article can be found online at https://doi.org/10.1016/j.fuel.2025.135851

Data availability

Data will be made available on request.

References

[1] Liss WR, Thrasher WH, Steinmetz GF, Chowdiah P, Attari A. Variability of natural gas composition in select major metropolitan areas of the United States. GRI Report 1992.
[2] Gassner G, Cenini P, Ulstein K. World's first ethane-powered marine vessels [Online]. Available: Wartsila 2016;20. https://www.wartsila.com/insights/article/worlds-first-ethane-powered-marine-vessels.
[3] Kobashi Y, Hirako S, Matsumoto A, Naganuma K. Flash boiling spray of diesel fuel mixed with ethane and its effects on premixed diesel combustion. Fuel 2019;237:686–93.
[4] Ahmad Z, Kaario O, Cheng Q, Larmi M. Impact of ethane enrichment on diesel-methane dual-fuel combustion. SAE Tech Pap 2020. 2020–01-0305.
[5] Ahmad Z, Kaario O, Karimkashi S, Qiang C, Vuorinen V, Larmi M. Effects of ethane addition on diesel-methane dual-fuel combustion in a heavy-duty engine. Fuel 2021;289:119834.
[6] Ulishney CJ, Dumitrescu CE. Optical investigation of methane, ethane, or propane and diesel at low load RCCI conditions. Fuel 2024;355:129472.
[7] Lowry W, de Vries J, Krejci M, Petersen E, Serinyel Z, Metcalfe W, et al. Laminar flame speed measurements and modeling of pure alkanes and alkane blends at elevated pressures. J Eng Gas Turb Pow 2011;133:9.

[8] Mitu M, Razus D, Giurcan V, Oancea D. Normal burning velocity and propagation speed of ethane–air: pressure and temperature dependence. Fuel 2015;147:27–34.
[9] Nilsson EJ, Van Sprang A, Larfeldt J, Konnov AA. The comparative and combined effects of hydrogen addition on the laminar burning velocities of methane and its blends with ethane and propane. Fuel 2017;189:369–76.
[10] Ravi S, Sikes TG, Morones A, Keesee CL, Petersen EL. Comparative study on the laminar flame speed enhancement of methane with ethane and ethylene addition. Proc Combust Inst 2015;35:679–86.
[11] Li J, Xie Y, Morsy M, Yang J. Laminar burning velocities, Markstein numbers and Cellular instability of spherically propagation ethane/hydrogen/air premixed flames at elevated pressures. Fuel 2024;364:131078.
[12] Zuo Z, Hu B, Bao X, Zhang S, Kong L, Deng L, et al. Quantitative research on cellular instabilities of premixed C1–C3 alkane–air mixtures using spherically expanding flames. Fuel Process Technol 2022;226:107075.
[13] Zuo Z, Hu B, Bao X, Zhang S, Fan L, Deng L, et al. Self-acceleration characteristics of premixed C1-C3 alkanes-air mixtures in a constant-volume chamber. Fuel Process Technol 2022;231:107252.
[14] Taamallah S, Vogiatzaki K, Alzahrani FM, Mokheimer EMA, Habib MA, Ghoniem AF. Fuel flexibility, stability and emissions in premixed hydrogen-rich gas turbine combustion: technology, fundamentals, and numerical simulations. Appl Energy 2015;154:1020–47.
[15] Chen L, Zhang R, Wei H, Pan J. Effect of flame speed on knocking characteristics for SI engine under critical knocking conditions. Fuel 2020;282:118846.
[16] Li J, Lu A, Xie Y, Yang J, Zhang C. Auto-ignition characteristics of coal-based naphtha. Appl Energy 2024;359:122768.
[17] Benbouaziz O, Mameri A, Hadef A, Aouachria Z. Characterization of biogas-syngas turbulent MILD combustion in the jet in hot co-flow burner. J Appl Fluid Mech 2021;14:1851–68.
[18] Belacel M, Hadef A, Mameri A, Tou I, Skender A, Salhi N. Statistical approach and numerical analysis of turbulent diffusion flame of CH_4/H_2 mixture. Energy Sources Part A: Recovery Util Environ. Eff. 2024;46:636–58.
[19] Hadef A, Mameri A, Tabet F, Aouachria Z. Numerical study of the impact of CO_2 dilution on emissions in turbulent diffusion flame. Energy Procedia 2017;139:273–9.
[20] Li J, Van Loo S, Yang J, Pekalski A. Turbulent flame acceleration and deflagration-to-detonation transitions in ethane–air mixture. Phys Fluids 2024;36:097115.
[21] Li J. Deflagration to detonation transition with increased reactivity of iso-octane and ethane mixtures [Phd thesis]. Leeds (UK): University of Leeds; 2024.
[22] Abdel-Gayed RG, Al-Khishali KJ, Bradley D. Turbulent burning velocities and flame straining in explosions. Proc R Soc Lond A 1984;391:393–414.
[23] Lawes M, Ormsby MP, Sheppard CGW, Woolley R. Variation of turbulent burning rate of methane, methanol, and iso-octane air mixtures with equivalence ratio at elevated pressure. Combust Sci Technol 2005;177:1273–89.
[24] Goulier J, Comandini A, Halter F, Chaumeix N. Experimental study on turbulent expanding flames of lean hydrogen/air mixtures. Proc Combust Inst 2017;36:2823–32.
[25] Kitagawa T, Nakahara T, Maruyama K, Kado K, Hayakawa A, Kobayashi S. Turbulent burning velocity of hydrogen–air premixed propagating flames at elevated pressures. Int J Hydrogen Energy 2008;33:5842–9.
[26] Wang S, Elbaz AM, Wang Z, Roberts WL. The effect of oxygen content on the turbulent flame speed of ammonia/oxygen/nitrogen expanding flames under elevated pressures. Combust Flame 2021;232:111521.
[27] Sierens R, Rosseel E. Variable composition hydrogen/natural gas mixtures for increased engine efficiency and decreased emissions. J Eng Gas Turbines Power 2000;122:135.
[28] Fairweather M, Ormsby MP, Sheppard CGW, Woolley R. Turbulent burning rates of methane and methane–hydrogen mixtures. Combust Flame 2009;156(4):780–90.
[29] Mandilas C, Ormsby MP, Sheppard CGW, Woolley R. Effects of hydrogen addition on laminar and turbulent premixed methane and iso-octane–air flames. Proc Combust Inst 2007;31:1443–50.
[30] Dai H, Wang J, Su S, Su L, Cai X, Huang Z. Turbulent burning velocity of hydrogen/n-heptane/air propagating spherical flames: effects of hydrogen content. Combust Flame 2024;260:113248.
[31] Wang S, Elbaz AM, Arab OZ, Roberts WL. Turbulent flame speed measurement of NH3/H2/air and CH4/air flames and a numerical case study of NO emission in a constant volume combustion chamber (CVCC). Fuel 2023;332:126152.
[32] Wang S, Elbaz AM, Wang G, Wang Z, Roberts WL. Turbulent flame speed of NH3/CH4/H2/H2O/air-mixtures: effects of elevated pressure and Lewis number. Combust Flame 2023;247:112488.
[33] Woolley RM, Fairweather M, Falle SAEG, Giddings JR. Prediction of confined, vented methane-hydrogen explosions using a computational fluid dynamic approach. Int J Hydrogen Energy 2013;38:6904–14.
[34] Damköhler G. The effect of turbulence on the flame velocity in gas mixtures. Zeitschr Elektrochem Angew Physikal Chem 1947;46. NACA-TM-1112.
[35] Clavin P, Williams FA. Theory of premixed-flame propagation in large-scale turbulence. J Fluid Mech 1979;90:589–604.
[36] Schmid HP, Habisreuther P, Leuckel W. A model for calculating heat release in premixed turbulent flames. Combust Flame 1998;113:79–91.
[37] Bradley D, Lau AKC, Lawes M. Flame stretch rate as a determinant of turbulent burning velocity. Philos Trans R Soc Lond A 1992;338:359–87.
[38] Bradley D, Lawes M, Mansour MS. Correlation of turbulent burning velocities of ethanol–air, measured in a fan-stirred bomb up to 1.2 MPa. Combust Flame 2011;158:123–38.
[39] Bradley D, Lawes M, Liu K, Mansour MS. Measurements and correlations of turbulent burning velocities over wide ranges of fuels and elevated pressures. Proc Combust Inst 2013;34:1519–26.
[40] Bradley D, Lawes M, Morsy ME. Measurement of turbulence characteristics in a large scale fan-stirred spherical vessel. J Turbul 2019;20:195–213.
[41] MATLAB 2021b, The MathWorks Inc., Natick, Massachusetts, 2021.
[42] Bradley D, Haq MZ, Hicks RA, Kitagawa T, Lawes M, Sheppard CGW, et al. Turbulent burning velocity, burned gas distribution, and associated flame surface definition. Combust Flame 2003;133:415–30.
[43] Vancoillie J, Sharpe G, Lawes M, Verhelst S. The turbulent burning velocity of methanol–air mixtures. Fuel 2014;130:76–91.
[44] Al-Khafaji M, Yang J, Tomlin AS, Thompson HM, de Boer G, Liu K. The measurement of turbulent burning velocities of methane-hydrogen-air mixtures at elevated pressures in a spherical vessel. Combust Flame 2025;272:113907.
[45] Borghi R, Escudie D. Assessment of a theoretical model of turbulent combustion by comparison with a simple experiment. Combust Flame 1984;56:149–64.
[46] Lipatnikov AN, Chomiak J. Turbulent flame speed and thickness: phenomenology, evaluation, and application in multi-dimensional simulations. Prog Energy Combust Sci 2002;28:1–74.
[47] Chen Z, Tang C, Fu J, Jiang X, Li Q, Wei L, et al. Experimental and numerical investigation on diluted DME flames: thermal and chemical kinetic effects on laminar flame speeds. Fuel 2012;102:567–73.
[48] Zhang W, Morsy ME, Ling Z, Yang J. Characterization of flame front wrinkling in a highly pressure-charged spark ignition engine. Exp Therm Fluid Sci 2022;132:110534.
[49] Bradley D, Lawes M, Mansour MS. Flame surface densities during spherical turbulent flame explosions. Proc Combust Inst 2009;32:1587–93.
[50] Creta F, Matalon M. Propagation of wrinkled turbulent flames in the context of hydrodynamic theory. J Fluid Mech 2011;680:225–64.
[51] Howarth TL, Hunt EF, Aspden AJ. Thermodiffusively-unstable lean premixed hydrogen flames: phenomenology, empirical modelling, and thermal leading points. Combust Flame 2023;253:112811.
[52] Chen Z, Burke MP, Ju Y. Effects of Lewis number and ignition energy on the determination of laminar flame speed using propagating spherical flames. Proc Combust Inst 2009;32:1253–60.
[53] Burke MP, Chen Z, Ju Y, Dryer FL. Effect of cylindrical confinement on the determination of laminar flame speeds using outwardly propagating flames. Combust Flame 2009;156:771–9.
[54] Zhang D, Liu J, Hou L. Experimental investigations of laminar and turbulent burning velocities of thermally cracked hydrocarbon fuels. Combust Flame 2022;245:112331.
[55] Abdel-Gayed RG, Bradley D, Lawes M. Turbulent burning velocities: a general correlation in terms of straining rates. Proc R Soc Lond A Math Phys Sci 1987;414:389–413.
[56] W.D. McComb, The physics of fluid turbulence, (1992). https://doi.org/10.1016/0010-4655(93)90157-8.
[57] Bradley D, Gaskell PH, Sedaghat A, Gu XJ. Generation of PDFS for flame curvature and for flame stretch rate in premixed turbulent combustion. Combust Flame 2003;135:503–23.
[58] Kheirkhah S, Gülder ÖL. Consumption speed and burning velocity in counter-gradient and gradient diffusion regimes of turbulent premixed combustion. Combust Flame 2015;162:1422–39.
[59] Shepherd IG. Flame surface density and burning rate in premixed turbulent flames. Symp (Int) Combust 1996;26:373–9.
[60] Sattler SS, Knaus DA, Gouldin FC. Determination of three-dimensional flamelet orientation distributions in turbulent V-flames from two-dimensional image data. Proc Combust Inst 2002;29:1785–92.